

OPEN ACCESS

LETTER



RECEIVED

3 October 2018

REVISED

18 December 2018

ACCEPTED FOR PUBLICATION

18 January 2019

PUBLISHED

8 February 2019

Original content from this work may be used under the terms of the [Creative Commons Attribution 3.0 licence](https://creativecommons.org/licenses/by/4.0/).

Any further distribution of this work must maintain attribution to the author(s) and the title of the work, journal citation and DOI.



Freestanding carbon nanomembranes and graphene monolayers nanopatterned via EUV interference lithography

Andreas Winter¹, Yasin Ekinci², Armin Götzhäuser³ and Andrey Turchanin^{1,4}

¹ Institute of Physical Chemistry, Friedrich Schiller University Jena, Lessingstr. 10, 07743 Jena, Germany

² Laboratory for Micro- and Nanotechnology, Paul Scherrer Institute, 5232 Villigen, Switzerland

³ Faculty of Physics, Bielefeld University, Universitätsstr. 25, 33615 Bielefeld, Germany

⁴ Abbe Center of Photonics (ACP), Albert-Einstein-Str. 6, 07745 Jena, Germany

E-mail: andrey.turchanin@uni-jena.de

Keywords: graphene, carbon nanomembrane, EUV interference lithography, nanoribbon, nanomesh

Supplementary material for this article is available [online](#)

Abstract

Two-dimensional materials, such as graphene, molecular nanosheets, hexagonal boron nitride or transition metal dichalcogenides have recently attracted substantial interest due to their potential use in electronics, chemical and biological sensors, nanooptics, and catalysis. For most of these applications, the functional nanostructures have to be prepared lithographically. In this respect, extreme ultraviolet interference lithography provides both high-resolution patterning with an ultimate limit in the sub-10 nm range and high throughput capability. Here we present the preparation of nanopatterned 1 nm thick freestanding molecular nanosheets—carbon nanomembranes (CNMs)—and single layer graphene employing this method and their characterization with a helium ion microscope. We demonstrate periodic arrays of suspended nanostructures of CNMs and graphene including nanoribbons with width between 20 nm and 500 nm and nanomeshes with openings between 140 nm and 300 nm and mesh lines down to 90 nm.

Introduction

Recent advances in the synthesis and transfer of two-dimensional (2D) materials have enabled the fabrication of macroscopically large though atomically thin freestanding nanosheets (see, e.g. [1, 2]). Therewith, perforated nanosheets have emerged as highly attractive materials for implementations in osmosis [3], fast material separation in the gaseous [4] and the liquid state [5, 6] as well as in studies of new physical phenomena including molecular translocation [7] or diffraction [8]. Despite these advances, the area of materials separation, for instance, is still dominated by macroscopically thick membranes [9], although nanomembranes of 2D materials can provide significantly higher mass transport rates and a lower energy consumption [10, 11]. One of the challenges here is the production of nanomembranes with well-defined nanopores including their shapes, sizes and spatial distribution. At present, mostly 2D nanomembranes with random nanopores have been investigated [12, 13], although regular nanopore arrays are advantageous for both fundamental studies and

applications [5]. For the generation of nanopores in 2D materials, electrochemical [14], plasma etching [15] techniques or block-copolymer templates [16] can be used; however, these techniques do not intrinsically provide any control over the spatial distribution or the precise shapes of the generated nanopores. While substantial progress has been made in nanopatterning of 2D materials on solid substrates (see, e.g. [17–19]), the preparing of nanopatterned suspended 2D materials remains challenging. Regular nanopore arrays in 2D materials can be produced with serial methods like focused ion beam (FIB) milling [5, 8, 20] or milling with a helium ion microscope (HIM) [21]; however, such serial methods only provide a limited throughput. Therefore, there is a high demand for new parallel methods to pattern 2D nanomembranes on the nanoscale, which also allow to form suspended 2D nanostructures.

Methods

In this work, we apply extreme UV interference lithography (EUV-IL) [22, 23] to pattern 2D

nanosheets and prepare their freestanding structures. Using a wavelength of 13.5 nm, EUV-IL enables a large area nanopatterning with sub-10 nm resolution [24] simultaneously being a highly parallel technique with a potential for high throughput nanofabrication [22, 23]. Employing EUV-IL, we nanopattern graphene monolayers grown by chemical vapor deposition (CVD) on Cu foils [25, 26] and carbon nanomembranes (CNMs) made by electron beam induced crosslinking of aromatic self-assembled monolayers [1], which are examples of ultimately thin carbon nanosheets. To this end, we apply resist-based patterning in combination with reactive ion etching (RIE) to introduce dot and hole patterns into CNMs and graphene and to engineer nanoribbons within dimensions from 20 to 500 nm. Subsequently, the generated nanostructures are prepared as freestanding objects on supporting grids. We characterize the supported and suspended nanostructures in CNMs and graphene with a HIM. This microscopy technique is especially well-suited for imaging 2D materials and in particular freestanding nanosheets as it provides high surface sensitivity, large depth of field and efficient charge compensation [27, 28].

A schematic representation of the fabrication of patterned nanosheets by EUV-IL is shown in figure 1. Initially, the graphene or CNM on a substrate is covered with a photoresist layer, figure 1(a). Subsequently, the sample is exposed to an interference pattern of EUV photons and the photoresist is developed, figures 1(b) and (c). Then, the photoresist pattern is transferred into the underlying 2D material via RIE, figure 1(e), and finally the resist is dissolved, figure 1(f). To form freestanding nanosheets, the patterned nanomembranes are transferred onto supporting substrates (e.g. grids) using the polymer assisted transfer [29, 30].

As EUV irradiation induces the crosslinking of the precursor self-assembled monolayers (SAMs) in a similar way as their irradiation with low-energy electrons [1], it was demonstrated in a previous work [31] that nanopatterned CNMs can be prepared in a resist-free process by means of EUV-IL. However, in this process very high irradiation doses of $\sim 50 \text{ J cm}^{-2}$ have to be applied [31]. These doses exceed the respective values for a typical photoresist by a factor of ~ 1000 [27]. Such long exposure times lead to blurring effects in the resulting structures due to a mechanical and thermal drift of the lithographic equipment over time, which restricts the achievable resolution and reproducibility as well as limits the throughput. By employing the patterning of a photoresist layer with subsequent pattern transfer by RIE, this effect can be significantly reduced. Note that also for graphene some resist-free nanopatterning techniques, e.g. based on atomic force microscopy (AFM) have been developed [32]. Although these techniques can provide a high resolution, their technological implementation is largely hindered due to their serial nature.

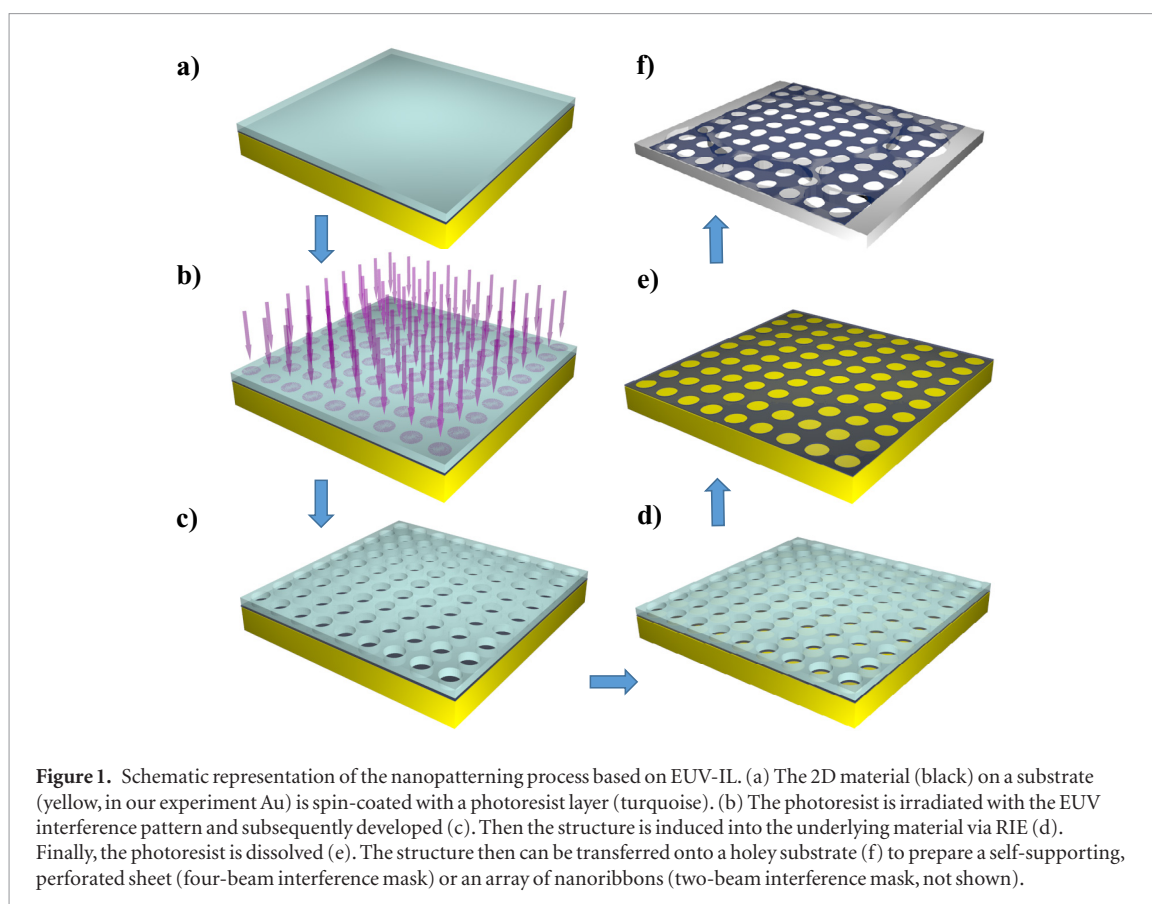
To obtain a reliable nanopatterning of CNMs and graphene, EUV irradiation doses were optimized for different EUV diffraction masks using poly (methyl methacrylate) (PMMA) as a photoresist. The optimized doses, evaluated from the pattern transfer into the photoresist, are listed in SI table 1, where they are also compared with the values required for the resist-free nanopatterning of CNMs with similar EUV diffraction masks. Typical doses for the resist-based nanopatterning were found to be in the range of 20–1000 mJ cm^{-2} , depending on the efficiency of the applied mask. Next, to achieve a reliable pattern transfer into the 2D materials via RIE, the respective doses were optimized considering such effects like a precise pattern transfer as well as modifications of the photoresist like its hardening or thinning. In this way, various nanostructures have been transferred into CNMs and graphene as reported below.

Experimental

To form SAMs, Au/mica substrates (300 nm, Georg Albert PVD) were introduced for 72 h into a $\sim 1 \text{ mM}$ solution of 4'-nitro-1,1'-biphenyl-4-thiol (NBPT, 99%, Taros) in N,N-dimethylformamide (DMF, Alfa Aesar, 99.8%, water free). After formation of the SAM, the samples were rinsed with DMF several times and blown dry in an argon stream. The formed SAM then was irradiated with electrons of 100 eV kinetic energy and a dose of 50 mC cm^{-2} under high vacuum conditions ($1 \times 10^{-8} \text{ mbar}$). This converts the SAM into a CNM by a well-established electron beam induced crosslinking process [33].

The graphene samples were grown in a CVD process on Cu foils (Alpha Aesar, thickness $25 \mu\text{m}$, 99.8%) in a tube furnace at $1 \times 10^{-3} \text{ mbar}$ base pressure (Gero F40-200) [25, 26]. The Cu foils were cleaned for 15 min in acetic acid (97%), for 1 min in isopropanol and subsequently were dried in an Ar stream. To remove the oxide layer from the substrate, they were annealed for 3 h at $1015 \text{ }^\circ\text{C}$ in a H_2 flow ($50 \text{ cm}^3 \text{ min}^{-1}$). To grow the graphene, a mixture of $70 \text{ cm}^3 \text{ min}^{-1} \text{ CH}_4$ (purity 4.5) and $10 \text{ cm}^3 \text{ min}^{-1} \text{ H}_2$ was introduced into the furnace for 15 min. For rapid cooling of the samples, the heating zone of the oven was moved away from the samples while keeping the precursor gases flowing.

To transfer graphene, an established PMMA assisted protocol was applied [29, 30]. To this end, a PMMA layer (100 nm, 50 kDa, All-Resist, AR-P 671.04) was spin coated onto the graphene/Cu foil samples and hardened for 10 min at $90 \text{ }^\circ\text{C}$. This procedure was followed by spin coating a second thicker PMMA layer (200 nm, 950 kDa, All-Resist, AR-P 679.04) and the subsequent hardening for 10 min at $90 \text{ }^\circ\text{C}$. To release the graphene, the Cu foil was etched by floating it for 3 h on a bath of ammonium persulfate solution (Sigma Aldrich, 2.5%). The etching step was followed by several washing steps with ultrapure



water to remove the residual etching solution. In order to perform EUV-IL, graphene samples were transferred either on flat SiO₂/Si or Au/mica substrates. The PMMA layer was removed by immersing the samples in acetone for 2 h.

The transfer of CNMs was carried out in the same way as for the graphene, however, a different etching solution (I₂/KI/H₂O in mass proportion of 1:4:10) was used to remove the Au layer. The Au layer was cleaved from mica in a well established process of water dipping of one of the sample edges [26].

To characterize the quality of graphene after the transfer, Raman spectroscopy has been conducted on graphene samples transferred on SiO₂. A typical Raman spectrum is shown in figure S1 (stacks.iop.org/TDM/6/021002/mmedia). A small D peak at the detection limit (D/G ~ 0.1) can be observed, indicating a low amount of microscopic defects in the graphene. The 2D/G ratio is ~2.4. The Raman spectra were taken in backscattering mode with a Bruker Senterra spectrometer. It was operated at with a frequency-doubled Nd:YAG laser at 532 nm, a 50 × objective and a thermoelectrically cooled CCD detector. The system's spectral resolution is 2–3 cm⁻¹. For peak shift calibration of the instrument, the Si peak at 520.7 cm⁻¹ was used.

The EUV-IL has been conducted at the beamline XIL-II of the Swiss Light Source. The beamline has an undulator source filtered by a pinhole to produce spatially coherent light with a wavelength of 13.5 nm, which allows for resolutions down to 7 nm [24, 34, 35]. For this technique, Cr transmission gratings on Si₃Ni₄

membranes were used to diffract the EUV beam. Their fabrication process is described elsewhere [22]. The masks carry two or four fields with gratings. The interference patterns of the diffracted beams were used to irradiate the samples, leading to line patterns and dot/hole patterns on an area of up to 1 × 1 mm². Especially for large area periodic structures, this technique is well suited. In this work, we have used standard photoresists to reduce limitations occurring when direct patterning methods are applied. As a positive-tone photoresist PMMA (600 kDa, AR-P 661.09, dissolved in chlorobenzene, All-Resist) and a high-resolution negative-tone photoresist hydrogen silsesquioxane (HSQ, XR-1541, Dow Corning) have been used. PMMA was spincoated at 3000 min⁻¹ for 45 s resulting in a thickness of about 1000 nm, while HSQ was spincoated at 5000 min⁻¹ for 60 s (thickness ~35 nm). These resist layers subsequently were patterned via EUV-IL with irradiation doses in the range of 20–100 mJ cm⁻². The resist layers were developed in methylisobutylketone (PMMA) or a NaOH buffered developer (HSQ, Microposit 351, Dow Corning), respectively. Structures in the photoresist subsequently were transferred into the respective 2D material via RIE in an oxygen plasma, while the photoresist layer afterwards was dissolved in acetone (PMMA) or a buffered oxide etch bath (HSQ), respectively.

For the preparation of freestanding nanostructures of CNMs and graphene, the samples (PMMA/CNM or PMMA/graphene) were placed on transmission electron microscopy grids (Cu 400 mesh, different

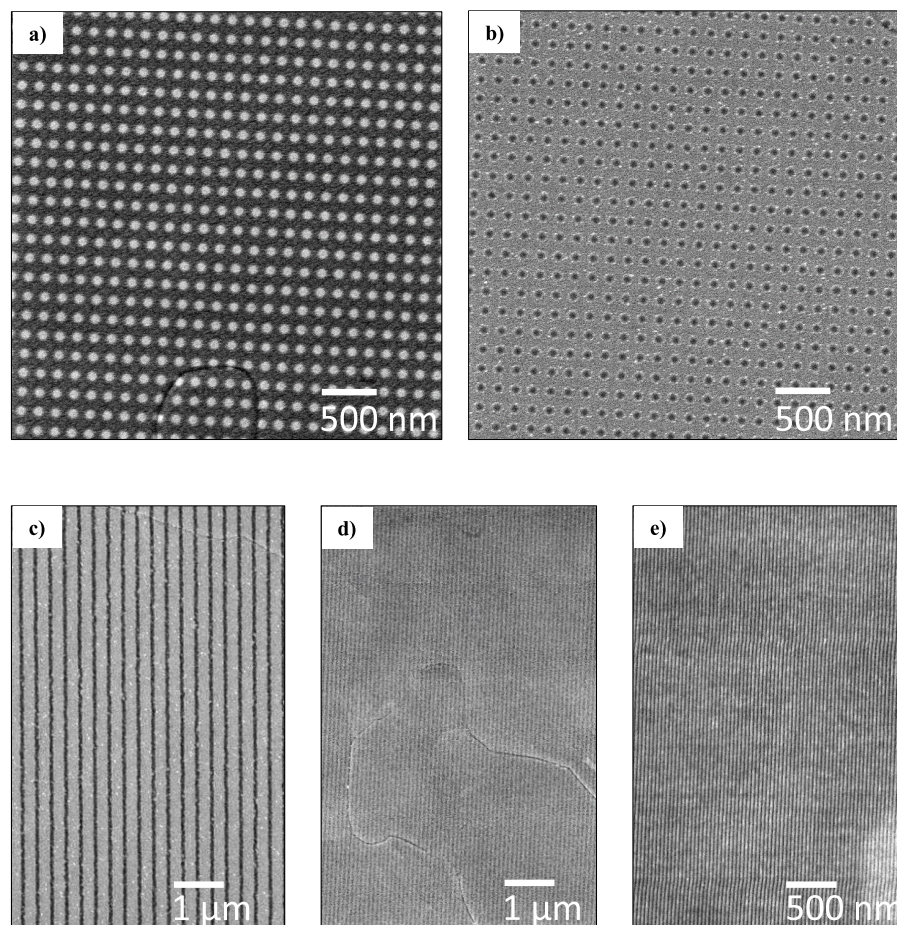


Figure 2. HIM images of different nanostructured CNMs on Au/mica: (a) 100 ± 10 nm holes in CNM with a periodicity of 225 ± 10 nm. (b) 100 ± 10 nm dots of CNM with the same periodicity and prepared with the same interference mask but using a different irradiation dose as in (a). (c) 125 ± 10 nm wide nanoribbons of CNM. (d) 50 ± 5 nm wide and (e) 22 ± 3 nm wide CNM nanoribbons. An image analysis shows low relative deviations of the structure sizes of $\sim 10\%$ for the structures in (d) and (e).

support films, Plano) using the same transfer protocol as for the transfer onto solid substrates. **The only difference in this process is that for the removal of the PMMA support film the acetone was exchanged with CO_2 in a critical point dryer (Autosamdri 815, Tousimis).** Using this method, ruptures in the samples can be avoided, which otherwise are known to occur due to the surface tension of the evaporating acetone.

The samples were imaged with a HIM (Orion plus, Carl Zeiss) at 35 kV using the secondary electron detector. An aperture of $10 \mu\text{m}$ with spot control 4 was used, resulting in beam currents of typically 5 pA. Most images were taken with line integration of 64 lines and an integration time of $1 \mu\text{s}$ at a working distance of 20 mm. Some images were also taken without an averaging mechanism and an integration time of $50 \mu\text{s}$.

Results and discussion

In the following, we present results on the fabrication and characterization of nanopatterned freestanding CNMs and graphene nanosheets. Figure 2 shows HIM images of some typical examples of CNMs patterned via EUV-IL with feature sizes varying from about 20

to 130 nm. In figures 2(a) and (b) we present structures where the same diffraction mask was used to prepare both a 100 nm hole pattern or a 100 nm dot pattern with a periodicity of 225 ± 10 nm each in CNMs by adjusting the irradiation dose from 20 mJ cm^{-2} to 40 mJ cm^{-2} . An example of a two-beam interference pattern, resulting in CNM nanoribbons of 125 ± 10 nm width having a periodicity of 350 ± 10 nm is shown in figure 2(c). For these structures, PMMA was employed as a photoresist. In order to obtain smaller structures, we employed HSQ as a standard negative photoresist established for high-resolution lithography [36]. Using HSQ, we were able to fabricate nanoribbon patterns of widths down to ~ 20 nm in CNMs (figures 2(d) and (e)). We have found that these nanoribbons possess a high mechanical stability and can be transferred onto arbitrary substrates including TEM grids, where they are freely suspended over large areas. Interestingly, we observed that the nanopatterns of CNMs on solid substrates typically showed some photoresist residues, whereas on the suspended CNM structures these are significantly reduced. **We attribute this observation to the fact that the photoresist from suspended nanostructures was**

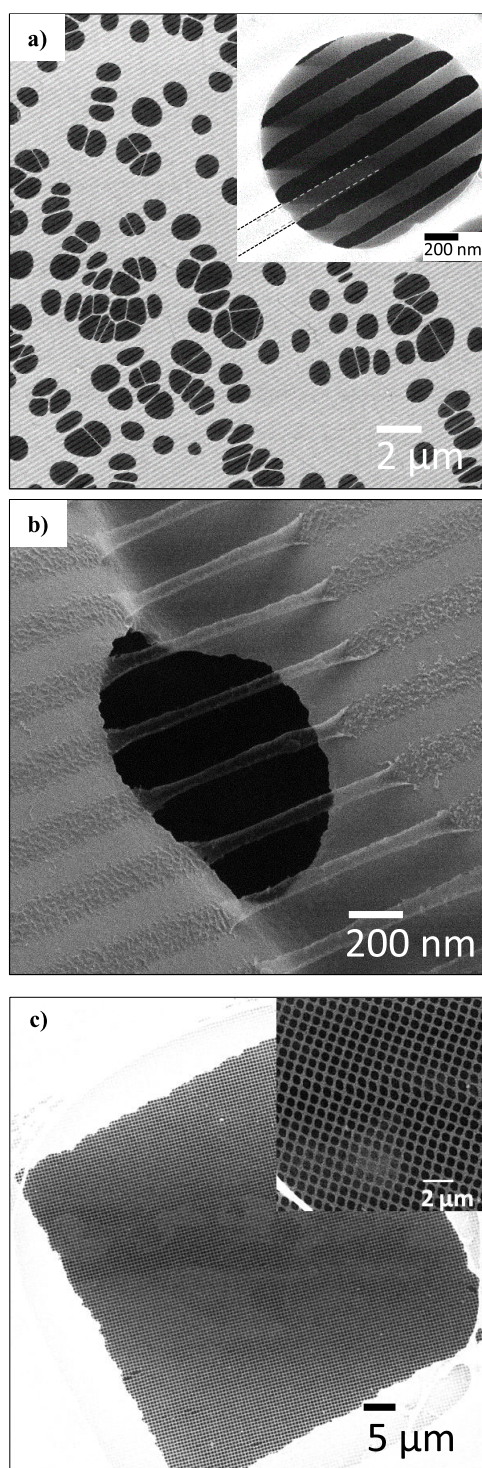


Figure 3. HIM images of nanostructured freestanding CNMs. (a) 150 ± 5 nm wide CNM nanoribbons transferred onto a TEM grid with a holey lacey carbon film. Freestanding areas appear darker in comparison to the lacey carbon substrate. Insert presents a magnified area with the freestanding nanoribbons. The freestanding nanoribbons appear narrower in comparison to the supported nanoribbons on the lacey carbon substrate. Dashed lines are included to guide the eye. (b) Similar CNM nanoribbons as in (a) on a curved lacey carbon substrate. (c) A square shaped CNM nanomesh of 260 ± 5 nm wide openings and 90 ± 5 nm wide mesh lines on a $50 \times 50 \mu\text{m}^2$ wide opening of a metal grid. The complete sample homogeneously covers about $1 \times 1 \text{ mm}^2$. Insert demonstrates the mesh with a higher magnification.

more effectively removed in a critical point dryer used for the preparation of freestanding nanosheets (see Experimental). Most probably, the treatment at the critical point of CO_2 promotes a more effective removal of photoresist residues. This observation may be of importance for a variety of applications, where transferred or nanopatterned 2D materials are used, e.g. in electronics and optoelectronics. This effect also was observed for the preparation of graphene nanostructures (see below).

After the pattern transfer, the feature sizes in the 2D materials were determined using standard image analysis software [37] and were compared to the corresponding feature sizes in the resist layer. Using an optimized RIE dose, no difference between the feature sizes in the photoresist and the 2D material was observed at the highest resolution of the HIM. We estimate the statistical error of these measurements to be ~ 3 nm. Moreover, the feature sizes are homogeneous over the entire area of $1 \times 1 \text{ mm}^2$ exposed to the EUV pattern. A statistical evaluation of different line and hole patterns shows that they can be produced with a standard deviation below 10 nm, independent of the measurement position and the type of features. Furthermore, the reproducibility of the pattern transfer between different samples was quantified in a statistical evaluation of different images, and the largest deviations were ± 10 nm. The edge sharpness of features was measured in line profiles of the microscopy images resulting in 8 ± 2 nm wide edges (15%–85% contrast value), independent of the feature sizes. Within this work, feature sizes between 22 nm and 500 nm have been realized. However, it has been found to be difficult to reach the resolution limit of the EUV-IL in the sub-10 nm range. Thus, we observed that the smallest studied features sized to 22 nm showed some inhomogeneity. We assume that the lithographic resolution can be further improved by optimizing the relevant parameters like, e.g. resist film thickness or the etching dose used for pattern transfer. However, as this work was not focused on the achievement of the highest resolution with EUV-IL but rather on the preparation of freestanding nanostructures of 2D materials, such an optimization was not performed.

Similar to the transfer of 2D materials onto solid substrates [29, 30], the prepared nanopatterns can be transferred onto supporting grids in order to produce freestanding structures. The smallest obtained freestanding features were 10 nm wide (see figures S2 and S3), while the openings in nanomeshes were varied between 140 nm and 300 nm with feature sizes down to 90 nm. Examples of freestanding CNM nanoribbons of 150 nm width as well as a square shaped CNM nanomesh of 260 ± 5 nm wide openings and 90 ± 5 nm wide mesh lines are shown in figure 3. It can be clearly seen from figure 3 that freestanding CNM nanostructures of well-defined shape can be prepared.

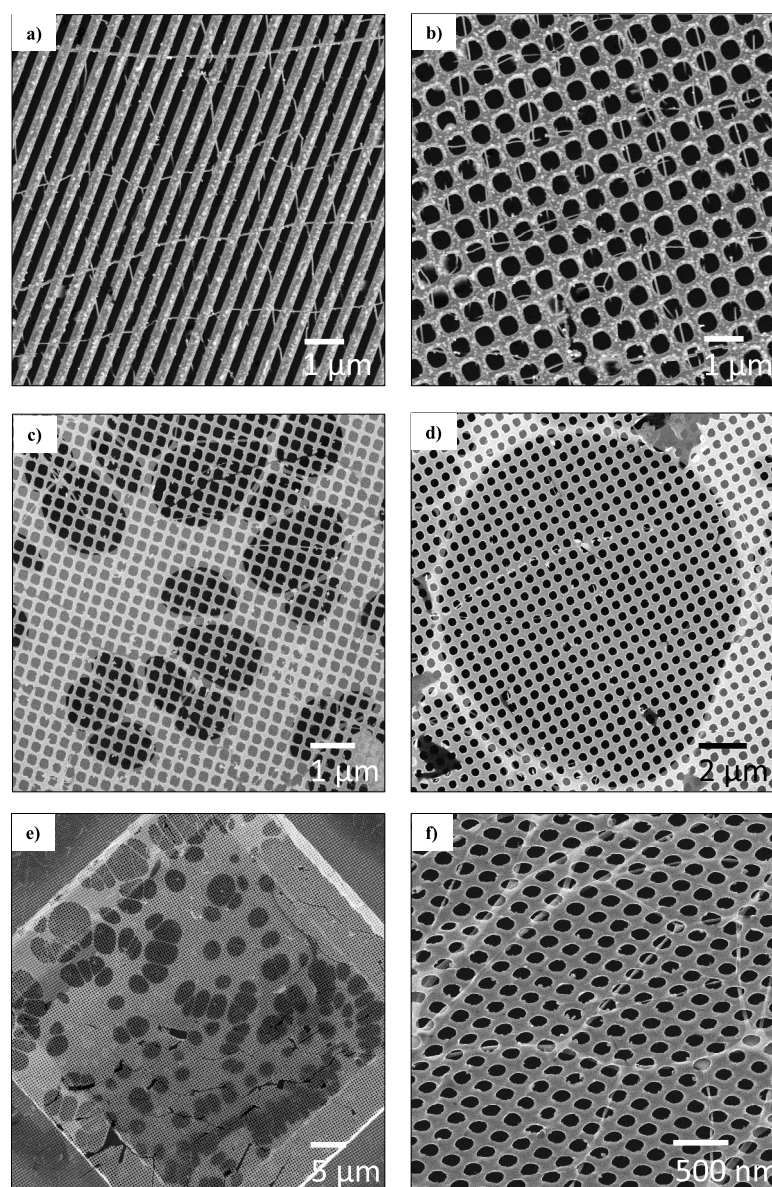


Figure 4. HIM images of nanostructured graphene: (a) nanoribbons of graphene on SiO₂ with 280 ± 10 nm width and 220 ± 10 nm distance. (b) Graphene nanomesh with 430 ± 10 nm circular openings and 110 ± 10 nm wide graphene features on SiO₂. (c)–(f) Freestanding graphene monolayers on holey lacy carbon support films. (c) Graphene nanomesh of 100 ± 10 nm width and 300 ± 10 nm spacing. (d) Graphene nanomesh with 260 ± 5 nm wide openings and graphene features of 240 ± 5 nm width. (e) Graphene nanomesh with 175 ± 5 nm wide openings and 90 ± 5 nm wide graphene features on an area of $50 \times 50 \mu\text{m}^2$. (f) Higher magnification of the image in (e). To provide better contrast, the image was taken at a detector angle of 45° . The feature size is very homogeneous over the whole sample. A statistical evaluation gives a standard deviation of only 6%.

Figures 3(a) and (b) show nanoribbons transferred onto a TEM grid with a holey lacy carbon support film. Figure 3(a) presents a pattern of parallel nanoribbons on the flat support (bright) and freestanding spanning the open areas (dark); the inset shows a high magnification image of freestanding nanoribbons. In figure 3(b) CNM nanoribbons are imaged on a curved supporting film. The 1 nm thick CNM nanomesh presented in figure 3(c) demonstrates a remarkable mechanical stability with an intact freestanding area of $2500 \mu\text{m}^2$ (with exception of a few point defects) supported by a $50 \mu\text{m} \times 50 \mu\text{m}$ metal grid. Note that in all HIM images, freestanding CNM areas appear darker in comparison to the supported areas, which can be especially well recognized in the inset to figure 3(a),

showing an increase of contrast towards the center of the freestanding nanoribbons. These imaging effects are related to the dielectric properties of the CNMs resulting in their electrostatic charging upon imaging with ions and therewith a lower yield of secondary electrons reaching the detector of the HIM [27].

As seen from figure 3(a) (inset), the width of the freestanding CNM nanoribbons is narrower in comparison to their original width on the carbon support film defined by lithography. As no rolling up at the edges of the ribbons is seen in this high resolution image, the difference in the width is representative for the residual strain ε in the membrane given by $\varepsilon = \frac{\Delta l}{L}$. From figure 3(a) and similar images of CNM nanoribbons with different width, a value

of $\varepsilon \approx 8\%$ – 10% was calculated. This value is higher than previously reported for the residual strain in CNMs [38, 39]. Using a Young's modulus of $E = 10$ GPa [38] and assuming a linear stress–strain relation, the residual stress $\sigma = \varepsilon \cdot E$ in the CNM nanoribbons can be estimated to be $\sigma \approx 1$ GPa. In figure 3(b) it is shown that due to the strain, a curved supporting substrate causes CNM nanoribbons to roll up. In the case of a 2D pattern (figure 3(c)), the width of the freestanding features in the open areas is slightly reduced revealing their residual strain. The residual strain in the CNMs is caused by their formation via electron beam induced crosslinking of the constituting molecules in a molecular monolayer. During this process, the molecules in the formed nanosheet form a network of new covalent bonds resulting in their spatial rearrangement and leading to reduced molecular distances within the CNM in comparison to the pristine monolayer [40].

Similar as for the supported nanostructures (see figure 2), a statistical evaluation of the feature sizes was conducted after the preparation of freestanding structures, showing no significant changes in their size distribution. The deviations between respective features are negligible, the variability between different samples is as low as ~ 5 nm and they show only small deviations from the intended structural dimensions also of ~ 5 nm. These results demonstrate that neither the pattern transfer by RIE nor the preparation of freestanding nanostructures change the absolute value or the variability of the feature sizes.

We found out that stacking of CNM nanoribbons allows to create even more complex freestanding structures based on the overlay of different nanopatterns. An example of such a structure is shown in figure S2, where two layers of CNM stripes are crossing at an angle of 30° . The stripes are 20 ± 5 nm wide and the resulting mesh has a width of 200×400 nm². This approach allows the preparation of various 2D structures not limited to the available interference patterns. Moreover, it was possible to prepare some special nanostructures of CNMs. Overexposure of 2D diffraction masks results in structures, which only in one direction are mechanically connected. In figure S3, we show an example of garland-like structures of CNMs, which in the narrowest regions are only 10 nm wide and still prove to be mechanically stable.

We also applied the developed methodology to nanopattern graphene as the ultimately thin nanosheet. CVD grown graphene monolayers on Cu foils were used. As the Cu foils have a relatively rough surface, the graphene was transferred on SiO₂ or Au substrates with lower substrate roughness (RMS 0.2 nm) for nanolithography. HIM images of nanostructured graphene on SiO₂ are shown in figures 4(a) and (b). **Similar to the CNM nanostructures, some residues of photoresist were found on these samples;**

however, as mentioned above, on the freestanding graphene sheets, after the treatment in a critical point dryer, these residuals have been significantly reduced.

It can be seen from figures 4(a) and (b) that the graphene nanoribbons and graphene nanomesh are superimposed with a web-like structure, which is due to folds in the graphene resulting from the transfer process. These features could not be completely eliminated via RIE, however, due to their low mechanical stability, they are not present in the freestanding structures (figures 4(c)–(f)). The graphene nanoribbons have a width of 280 nm with 220 nm spacing while the circular holes in the graphene nanomesh are 430 nm wide with a distance of 570 nm between their centers. An analysis of the feature sizes gives a standard deviation of 10 nm.

To prepare freestanding graphene structures, nanopatterned samples have been transferred onto supporting grids. In figures 4(c)–(f), we show some examples of such freestanding nanostructures. In figure 4(c), a square shaped graphene nanomesh with 100 nm line width and 300 nm wide openings is presented. The standard deviation of the feature sizes is about 10 nm. A graphene mesh with circular openings of 260 ± 5 nm is shown in figure 4(d). The shortest distance between two adjacent openings is 240 ± 5 nm. Figure 4(e) shows that such graphene nanomeshes can span a supporting grid over large areas of ~ 2500 μm^2 showing only some minor cracks due to the brittleness of the graphene. The standard deviation of the pore sizes, as well as the deviation from the intended feature sizes, was measured to be ~ 5 nm. Such structures are found to have a homogeneous pore size distribution over the whole structured area of 1×1 mm². For these samples, the feature sizes are found to be remarkably homogeneous. An analysis of the structure shown in figure 4(f) with circular graphene openings of 175 ± 5 nm gives a relative standard deviation of only 6%. In comparison to the freestanding CNM nanostructures, we do not observe any shrinkage in the freestanding graphene structures. We attribute this observation to the higher Young's modulus of graphene of 1 TPa [41], which reduces the influence of possible residual stress in the graphene nanostructures on their geometrical shape.

Summary

In summary, we have demonstrated the application of extreme UV interference lithography (EUV-IL) for the nanopatterning of 1 nm thick molecular nanosheets (CNMs) as well as single layer graphene. The resulting perforated nanosheets and nanoribbons can be prepared as supported films on solid substrates as well as freestanding objects on holey supports and grids. The developed EUV-IL procedures enable the patterning of these 2D materials with periodic features of sizes ranging from 20 to 500 nm.

Helium ion microscopy is well suited for a detailed characterization of the created nanopatterns. CNM and single layer graphene nanostructures could be produced over areas of $\sim 1 \times 1 \text{ mm}^2$ with an accuracy of 5–10 nm. Suspended nanoribbons have been prepared with feature sizes down to 20 nm, while the smallest openings in nanomeshes were 140 nm wide. The freestanding nanostructured CNMs and graphene sheets show a remarkably high mechanical stability and can span areas of up to $\sim 2500 \mu\text{m}^2$. The developed methodology paves the way for the implementation of freestanding nanopatterned 2D materials in devices. This is not restricted to carbon-based materials but can be extended to a variety of other inorganic (e.g. MoS₂, hBN) and organic (e.g. 2D polymers, metal-organic frameworks) nanosheets.

Acknowledgments

Financial support of the Deutsche Forschungsgemeinschaft (DFG) through research grants TU149/2-2, TU149/5-1, TU149/8-2, DFG TRR 234 ‘CataLight’ (B7 and Z2) as well as research infrastructure grant INST 275/257-1 FUGG is acknowledged. We also thank the Volkswagenstiftung for financial support through grant I/85119.

ORCID iDs

Andrey Turchanin  <https://orcid.org/0000-0003-2388-1042>

References

- [1] Turchanin A and Götzhäuser A 2016 *Adv. Mater.* **28** 6075
- [2] Boutilier M S H, Jang D, Idrobo J-C, Kidambi P R, Hadjiconstantinou N G and Karnik R 2017 *ACS Nano* **11** 5726
- [3] Feng J, Graf M, Liu K, Ovchinnikov D, Dumcenco D, Heiranian M, Nandigana V, Aluru N R, Kis A and Radenovic A 2016 *Nature* **536** 197
- [4] Jiang D-E, Cooper V R and Dai S 2009 *Nano Lett.* **9** 4019
- [5] Celebi K, Buchheim J, Wyss R M, Droudian A, Gasser P, Shorubalko I, Kye J-I, Lee C and Park H G 2014 *Science* **344** 289
- [6] Yang Y *et al* 2018 *ACS Nano* **12** 4695
- [7] Schneider G F, Kowalczyk S W, Calado V E, Pandraud G, Zandbergen H W, Vandersypen L M K and Dekker C 2010 *Nano Lett.* **10** 3163
- [8] Brand C *et al* 2015 *Nat. Nanotechnol.* **10** 845
- [9] Choi J, Roychowdhury A, Kim N, Nikitopoulos D E, Lee W, Han H and Park S 2010 *J. Micromech. Microeng.* **20** 085011
- [10] Zhao Y, Xie Y, Liu Z, Wang X, Chai Y and Yan F 2014 *Small* **10** 4521
- [11] Drioli E, Ali A and Macedonio F 2015 *Desalination* **356** 56
- [12] Koenig S P, Wang L, Pellegrino J and Bunch J S 2012 *Nat. Nanotechnol.* **7** 728
- [13] O’Hern S C, Stewart C A, Boutilier M S H, Idrobo J-C, Bhaviripudi S, Das S K, Kong J, Laoui T, Atieh M and Karnik R 2012 *ACS Nano* **6** 10130
- [14] Feng J *et al* 2015 *Nano Lett.* **15** 3431
- [15] Surwade S P, Smirnov S N, Vlasiouk I V, Unocic R R, Veith G M, Dai S and Mahurin S M 2015 *Nat. Nanotechnol.* **10** 459
- [16] Kim M, Safron N S, Han E, Arnold M S and Gopalan P 2010 *Nano Lett.* **10** 1125
- [17] Sandner A, Preis T, Schell C, Giudici P, Watanabe K, Taniguchi T, Weiss D and Eroms J 2015 *Nano Lett.* **12** 8402
- [18] Ding J, Du K, Wathuthanthri I, Choi C-H, Fisher F T and Yang E-H 2014 *J. Vac. Sci. Technol. B* **32** 06FF01
- [19] Mackenzie D M A, Smistrup K, Whelan P R, Luo B, Shivayogimath A, Nielsen T, Petersen D H, Messina S A and Boggild P 2017 *Appl. Phys. Lett.* **111** 193103
- [20] Kotakoski J, Brand C, Lilach Y, Cheshnovsky O, Mangler C, Arndt M and Meyer J C 2015 *Nano Lett.* **15** 5944
- [21] Emmrich D, Beyer A, Nadzeyka A, Bauerdick S, Meyer J C, Kotakoski J and Götzhäuser A 2016 *Appl. Phys. Lett.* **108** 163103
- [22] Auzelyte V *et al* 2009 *J. Micro/Nanolith. MEMS MOEMS* **8** 021204
- [23] Mojarad N, Hojeij M, Wang L, Gobrecht J and Ekinci Y 2015 *Nanoscale* **7** 4031–7
- [24] Päivänranta B, Langner A, Kirk E, David C and Ekinci Y 2011 *Nanotechnology* **22** 375302
- [25] Li X *et al* 2009 *Science* **324** 1312
- [26] Woszczyna M, Winter A, Grothe M, Willunat A, Wundrack S, Stosch R, Weimann T, Ahlers F and Turchanin A 2014 *Adv. Mater.* **26** 4831
- [27] Beyer A, Vieker H, Klett R, Meyer zu Theenhausen H, Angelova P and Götzhäuser A 2015 *Beilstein J. Nanotechnol.* **6** 1712–20
- [28] Hlawacek G and Götzhäuser A 2016 *Helium Ion Microscopy* (Berlin: Springer)
- [29] Turchanin A, Beyer A, Nottbohm C T, Zhang X, Stosch R, Sologubenko A, Mayer J, Hinze P, Weimann T and Götzhäuser A 2009 *Adv. Mater.* **21** 1233
- [30] Götzhäuser A, Nottbohm C and Beyer A 2007 Method for transferring a monolayer *European Patent* 2144711, *US Patent* 8377243 B2, 11
- [31] Schnietz M, Turchanin A, Nottbohm C T, Beyer A, Solak H H, Hinze P, Weimann T and Götzhäuser A 2009 *Small* **5** 2651
- [32] Jiang Y, Sun Y and Song J 2017 *Micron* **97** 29
- [33] Turchanin A, Käfer D, El-Desawy M, Wöll C, Witte G and Götzhäuser A 2009 *Langmuir* **25** 7342
- [34] Solak H H, David C, Gobrecht J, Wang L and Cerrina F 2002 *Microelectron. Eng.* **61** 77
- [35] Karim W, Tschupp S A, Oezaslan M, Schmidt T J, Gobrecht J, van Bokhoven J A and Ekinci Y 2015 *Nanoscale* **7** 7386
- [36] Ekinci Y, Solak H H, Padeste C, Gobrecht J, Stoykovich M P and Nealey P F 2007 *Microelectron. Eng.* **84** 700
- [37] Rasband W 2016 *ImageJ*, Version 1.51
- [38] Zhang X, Waitz R, Yang Y, Lutz C, Angelova P, Götzhäuser A and Scheer E 2015 *Appl. Phys. Lett.* **106** 063107
- [39] Zhang X, Neumann C, Angelova P, Beyer A and Götzhäuser A 2014 *Langmuir* **30** 8221
- [40] Matei D G *et al* 2013 *Adv. Mater.* **25** 4146
- [41] Lee C, Wei X, Kysar J W and Hone J 2008 *Science* **321** 385